NASA Technical Memorandum 110329

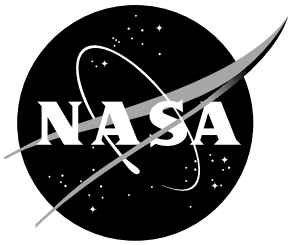

Subsonic Dynamics of Stardust Sample Return Capsule

R. A. Mitcheltree and C. M. Fremaux
Langley Research Center, Hampton, Virginia

March 1997

National Aeronautics and
Space Administration
Langley Research Center
Hampton, Virginia 23681-0001

Subsonic Dynamics of Stardust Sample Return Capsule

R. A. Mitcheltree *, and C. M. Fremaux †
NASA Langley Research Center, Hampton, Virginia

Abstract

Subsonic dynamic stability tests performed in the NASA Langley 20-Foot Vertical Spin-Tunnel on a 0.238 scale model of the Stardust Sample Return Capsule are discussed. The tests reveal that the blunted 60 degree half-angle cone capsule is dynamically unstable at low subsonic conditions due to the aft location of the center-of-gravity (0.351 body diameters back from the nose). The divergent behavior of the capsule continued when the center-of-gravity was moved to 0.337 and 0.313 body diameters back from the nose. When the center-of-gravity was moved further forward to 0.290 body diameters back from the nose, the vehicle established itself in a limit cycle with amplitude around 10 degrees. Two afterbody modifications were examined which proved unsuccessful in alleviating the instability of the original design. Finally, the addition of different sized parachutes was examined as a means to stabilize the vehicle. The parachute tests indicate that a parachute with equivalent full scale drag area of at least 2.24 ft^2 is necessary to assure large perturbations are damped.

Nomenclature

A = area, ft^2
A_p = parachute area, ft^2
C_A = axial force coefficient
C_N = normal force coefficient
C_m = moment coefficient referenced to the nose
$C_{m,\alpha}$ slope of the moment coefficient with respect to angle-of-attack, deg^{-1}
D = maximum body diameter, ft
I_x = moment of inertia about the x-axis, $slug - ft^2$
I_y = moment of inertia about the y-axis, $slug - ft^2$
I_z = moment of inertia about the z-axis, $slug - ft^2$
M = Mach number
N = model to vehicle length scale factor
q_∞ = free-stream dynamic pressure, lb/ft^2
Re_D = Reynolds number based on diameter
t = time, sec
V = freestream velocity, ft/s
x, y, z = coordinate directions, ft
$x_{c.g.}$ = distance center-of-gravity is aft of nose, ft
α = angle-of-attack, $deg.$
β = angle-of-sideslip, $deg.$
σ = ratio of air density at altitude to that at sea level
ν = kinematic viscosity at altitude, ft^2/s^2
ν_0 = kinematic viscosity at sea level, ft^2/s^2
ω = average oscillation frequency, rad/s

*Aerospace Engineer, Aerothermodynamics Branch, Aero- and Gas Dynamics Division, NASA Langley Research Center.
†Aerospace Engineer, Vehicle Dynamics Branch, Flight Dynamics and Control Division, NASA Langley Research Center.

Table 1: Target Mass Properties

	Weight (lb)	Ix (slug-ft^2)	Iy (slug-ft^2)	Iz (slug-ft^2)	$x_{c.g.}/D$
Flight	90.6	1.62	1.31	1.26	0.351
Model	1.66	1.68 $\times 10^{-3}$	1.36 $\times 10^{-3}$	1.30 $\times 10^{-3}$	0.351

Introduction

Stardust[1], the fourth Discovery-class mission, is scheduled for launch in February of 1999. In addition to collecting interstellar dust, the robotic spacecraft will fly within 100 km of the comet Wild-2 nucleus and collect material from the coma parent-molecular zone. These materials will be returned to Earth for sub-micron level analysis. To accomplish this objective, a capsule containing the collected particles must safely transit an intense Earth entry, descent, and landing. This paper focuses on the aerodynamics of the Stardust Sample Return Capsule (SRC) during the terminal subsonic portion of that entry. The results also have relevance to other proposed sample return missions.

The entry of the Stardust SRC at 12.6 km/s will be the fastest Earth entry ever attempted. Its trajectory traverses the hypersonic-rarefied, hypersonic-continuum, supersonic, transonic, and subsonic flow regimes. The passive capsule, once released from its host bus, will rely solely on the predetermined balance between aerodynamic forces and gravity to decelerate it through the atmosphere to a parachute landing in the Utah Test Landing Range. Reference 2 discusses the static aerodynamics of the capsule over the entire speed range. This paper attempts to predict the subsonic dynamic performance of the capsule.

As the planetary-entry probes for Mars Viking, Pioneer-Venus, and Galileo-Jupiter were being designed in the late 1960's and early 1970's, the subsonic-dynamic performance of blunt bodies similar to the 60 degree half-angle cone proposed for the Stardust SRC were studied in the vertical wind tunnel[3–7] at NASA Langley. Similar studies were also conducted in horizontal wind tunnels[8,9], drop tests[10,11], flight tests[12], ballistic ranges[13], and in theoretical simulations[14,15]. As the erratic dynamic behavior of high-drag bodies in subsonic and transonic flows was revealed, planetary mission designers chose to avoid these flight regimes by deploying parachutes at supersonic speeds. The Stardust SRC is designed to land in a 75-km major-axis elliptical target area in the Utah Test Landing Range. To facilitate this landing, drift due to surface winds must be minimized. A decision was made to delay parachute deploy until Mach 0.16 and 10,000 feet altitude. This decision requires the capsule to possess sufficient subsonic aerodynamic stability to maintain a controlled attitude through this flight regime for successful parachute deployment.

The purpose of this paper is to document subsonic dynamic stability tests performed in the NASA Langley 20-Foot Vertical Spin Tunnel. Variation in dynamic stability of the Stardust SRC as a function of center-of-gravity (c.g.) location is explored. Two afterbody modifications are examined in an attempt to alter the stability. Finally, the addition of different sized parachutes is examined as a means to stabilize the vehicle.

Sample Return Capsule Geometry and Models

The forebody geometry of the SRC is a 60-degree half-angle sphere-cone with nose radius equal to 9.0 in, shoulder radius of 0.75 in, and overall diameter of 32.0 in. The afterbody shape is a 30-degree cone which terminates in a flat stern whose radius is 8.33 in. (Note, the afterbody of the SRC has since been shortened by 1.7 in. The vehicle's length from nose to stern is now 19.6 in. Dynamic stability is not sensitive to small changes in afterbody shape[3,6,9]. Therefore, the present results should be applicable to this shorter afterbody.)

The 23.8 percent dynamically scaled model is constructed of high density foam and fiberglass for testing in the spin tunnel. The geometry is shown in Fig. 1. A comparison of the mass properties of the model (target values) and the expected flight values is given in Table 1. The model is constructed with means to vary the c.g. location and is ballasted to represent the vehicle at an altitude of 10,000 feet. Model values given in Table 1 are for the configuration with the c.g. location of 0.351 body-diameters (D) back from the nose. Mass properties for each of the c.g. locations are given in Table 4 of the *Results* section. The geometry of afterbody modifications and parachutes are presented in the *Results* section.

Spin Tunnel and Dynamic Scaling

The Langley 20-Foot Vertical Spin Tunnel is an atmospheric, annular return, vertical wind tunnel. The test section is 20 feet across and 25 feet in length. A 400 hp electric motor (1300 hp for short periods) turns a 3-bladed, fixed pitch fan to produce speeds of up to 90 ft/s, with a maximum acceleration and deceleration capability of 15 ft/s^2 and 25 ft/s^2, respectively. Figure 2 represents a cross-section of the facility. The axis system and aerodynamic angle definitions used in Spin Tunnel testing are shown in Fig. 3. A complete description of the Spin Tunnel may be found in Ref. 16.

For the Stardust tests, a lightweight tether system was used to reduce model damage from impact with the tunnel walls. A smooth metal ring was suspended in the center of the test section using guy wires. The tether was attached to the rear face of the afterbody, routed through the metal ring, and attached to the tunnel wall. At the beginning of a test, the model was suspended on the tether with the tunnel fan stopped. As the tunnel was brought up to speed, the tether became slack when model drag equaled the model weight (see Fig. 2). The tether appeared to have little influence on the model motions.

Standard videotapes are made to document each test and aid in qualitative analysis. However, primary data for tests of free-flying models are 6 degree-of-freedom (6 DOF) motion time histories, obtained via the Spin Tunnel Model Space Positioning System (MSPS). The MSPS is a non-intrusive, computer workstation-based system that uses a single video camera view of retro-reflective targets attached to known locations on a model to generate post-test estimates of model attitude and position at a sample rate of 60 Hz. Numerical differentiation of attitude time histories is used to calculate rates and accelerations. Typically, the accuracy of quantities reported by MSPS is within plus or minus one degree of the actual values. However, due to the small size of the Stardust SRC model (diameter one half to one third the span of a typical airplane model), the accuracy of the system was degraded. No error analysis for the current tests was performed, but it is believed that the angle values reported in this document are to within plus or minus two degrees.

Data acquisition using the MSPS system begins at a time specified by the operator during a test run. As such, the beginning of the plots (t=0) contained in this report corresponds to an arbitrary point in the test. The end of the data trace occurs when the retro-reflective targets are no longer in the camera field of view. For the present tests, loss of track occurred when the model was rolled or pitched to such a large angle that the targets were no longer visible. It should be noted, however, that the end of the plotted data sequence does not necessarily correspond to the time when an oscillation became divergent. Visual review of the corresponding test videotape is used to supplement the data provided by MSPS for this purpose. Reference 17 provides further discussion of the MSPS system.

Test section velocity is obtained using pitot-static pressure probes as well as a temperature probe protruding from the tunnel walls. The calculated airspeed is used to determine the equilibrium sink rate of the free-flying model.

Free flying models tested in the Spin Tunnel are dynamically scaled using the dynamic scaling parameters in Table 2. The dimensions of mass, length, and time are scaled so that the model results may be applied directly to predict the behavior of the full-scale vehicle. In this process, time is scaled on the basis of equal Froude number, length on the basis of similar geometry, and mass properties by assuming equal relative density, (i.e., the ratio of vehicle density to air density at the desired altitude). Model values are obtained by multiplying full-scale values by the listed scale factors. A detailed discussion of dynamic scaling may be found in Ref. 18.

Subsonic Static Aerodynamics

A horizontal wind tunnel investigation of the static subsonic aerodynamics of a 0.30 scale Stardust SRC model was conducted at Mach 0.16[2]. The tests were conducted in the ViGYAN Low Speed Wind Tunnel in Hampton, Virginia. This tunnel is a conventional, straight-through, open-return type layout with a 3 by 4 ft. entrance jet and an open test section. The tunnel was run at a dynamic pressure of 0.018 atm. The expected flight dynamic pressure is 0.012 atm. Reynolds numbers based on diameter (Re_D) for the tests were 0.9×10^6, the expected flight value is near 2.0×10^6. The question as to the nature of the boundary layer for the flight case was not answered, nor is it known if the wind tunnel test case was turbulent.

The measured aerodynamic coefficients are listed in Table 3. The normal-force and moment coefficients may be considered linear over the angle-of-attack range examined with slopes 0.0031 deg^{-1} and -0.00276 deg^{-1} respectively. Moment coefficients are referenced about the actual nose of the vehicle. The center-of-pressure for

Table 2: Dynamic Scaling Relationships used in Stardust SRC tests.

Parameter	Scale Factor
Linear Dimension	N
Relative Density	1
Froude Number	1
Mass	N^3/σ
Moment of Inertia	N^5/σ
Linear Velocity	$N^{1/2}$
Linear Acceleration	1
Angular Velocity	$1/N^{1/2}$
Time	$N^{1/2}$
Reynolds Number	$N^{3/2}\nu/\nu_0$

Table 3: Subsonic Static Aerodynamics (M = 0.16).

α	C_A	C_N	C_m
0.00	0.8739	0.0000	0.0000
2.02	0.8759	0.0053	-0.0058
4.00	0.8779	0.0119	-0.0115
6.04	0.8794	0.0177	-0.0171
7.99	0.8809	0.0242	-0.0227
12.02	0.8838	0.0357	-0.0332
16.01	0.8822	0.0485	-0.0446
20.00	0.8774	0.0613	-0.0573
24.01	0.8607	0.0723	-0.0676
28.01	0.8212	0.0855	-0.0757

this configuration is 0.89 D back from the nose. Since the expected c.g. for the SRC is 0.35 D back from the nose, the vehicle is statically stable.

Results

Results from the NASA 20-Foot Vertical Spin Tunnel tests are reported in four sections. The first section describes the stability of the baseline geometry as a function of c.g. location. Next, comments on Reynolds number effects are presented. Two afterbody modifications are then examined. Finally, results from the parachute tests are presented. Figure 3 presents the axis system and aerodynamic angle definitions used in subsequent figures.

Dynamic Stability of the Baseline Geometry

A summary of the baseline geometry's results are presented in Table 4. Tests with the model's c.g. at the expected flight location of 0.351 body-diameters (D) back from the nose reveal that the configuration is dynamically unstable. Without external excitation, the amplitude of oscillations quickly increase until either the tunnel dynamic pressure no longer supports the model (drag decreases with angle-of-attack), or the motion diverges and the model tumbles. A representative attitude time history for one run is presented in Fig. 4.

Similar divergent behavior is observed for c.g. locations at 0.337 D and 0.313 D back from the nose. Representative time histories for those two cases are presented in Figs. 5 and 6. Comparisons of the figures may provide an indication of the relative degree of instability present in each case. However, review of the videotapes reveals that oscillation growth rates varied widely for a given configuration. The plots are a single time history

Table 4: Summary of Baseline Geometry Tests (as tested full scale equivalent values)

test number	center of gravity position	weight, lb,	I_x, slug-ft^2	I_y, slug-ft^2	I_z, slug-ft^2	comments
1	0.351 D	90.6	1.64	1.32	1.24	oscillations rapidly diverged
2	0.337 D	90.4	1.66	1.28	1.23	oscillations rapidly diverged
3	0.313 D	89.7	1.64	1.33	1.25	oscillations diverged
4	0.290 D	90.6	1.48	1.30	1.25	oscillations limit cycle +/- 10^0
5	0.290 D	90.6	1.48	1.30	1.25	model perturbed during test: limit cycle remains
6	0.290 D	90.6	1.48	1.30	1.25	model prerotated limit cycles amplitude increases

from the MSPS system taken during a single run. In general, if the oscillations were divergent, little quantitative data can be extracted from the time histories.

With the c.g. location at 0.290 D, the stability of the configuration is improved significantly. This location is approaching the maximum diameter of the model which is 0.26 D back from the nose. As shown in Fig. 7, the model's attitude behavior is characterized by limit-cycle oscillations in angles of attack and sideslip, with a maximum amplitude of less than 10^0. These observations are consistent with Bendura's results of Ref. 3. In that reference, sharp-shouldered, 60^0 half-angle cones with a flat base and with a small conical afterbody were examined. Center-of-gravity locations in those tests varied between 0.101 and 0.273 D which is much closer to the nose than the range examined in the present tests. All of the Bendura configurations were dynamically stable, but with decreasing stability with aft movement of the c.g. Extrapolating his results leads to a conclusion consistent with the present observations that instability results when the c.g. location is more than 0.30 D back from the nose.

Two additional tests were conducted with the c.g. location 0.290 D configuration. In the first, the model was intentionally perturbed to near 30 degrees angle of attack during the run. This induced oscillation did not grow but decreased to the 10^0 limit cycle observed earlier. In the second, the model was spun at approximately 60 rpm while hanging from the tether, then the tunnel velocity was brought to speed. The spin rate decayed during the test to approximately 10 rpm. It is difficult to make quantitative measurements of the effect of spin rate, however, it appeared that the amplitude of the oscillations were larger for the spinning model than in the original non-rotating tests. This observation is consistent with that of Ref. 11 which examined the effect of large spin rates on entry body's dynamic stability in the terminal flight regime.

An attempt was also made to assess the configuration's stability in a backwards orientation (using the configuration from test 1 in Table 4). The maximum tunnel velocity was insufficient to fully support the model in this orientation. However, by allowing the model to slowly descend through the test section, a short test time without tether tension was achieved. During this period, the model appeared to be stable backwards.

Table 5: Comparison of static pitch stability derivatives

center of gravity position	$C_{m,\alpha}$ from static tests, deg^{-1} ($Re_D = 0.9 \times 10^6$)	$C_{m,\alpha}$ from dynamic tests, deg^{-1} ($Re_D = 0.3 \times 10^6$)
0.290 D	-0.0019	-0.0020
0.313 D	-0.0018	-0.0018
0.337 D	-0.0017	-0.0016
0.351 D	-0.0017	-0.0019

Reynolds Number Effects

The Reynolds number based on diameter (Re_D) for these tests is 0.3×10^6. The flight value is as large as 2.2×10^6. The Spin Tunnel is not capable of performing an independent variation of Re_D. In an attempt to simulate the higher Re_D associated with the flight case, two different boundary-layer strakes were installed on the 0.351 D c.g. configuration. The circumferential strakes extended out from the model at its maximum diameter for a distance of 5 percent of the diameter. The first was a knife-edge strake. The second was serrated with 60 degree triangles. While some variation in the rate of oscillation growth was observed with the strake additions, both continued to diverge in a manner similar to the non-straked tests of test 1.

Further insight into potential Reynolds number effects on dynamic stability may be gained by comparing the static stability characteristics of the configuration at different conditions. Similarity of static stability characteristics at different Re_D does not guarantee that the dynamic behavior will be identical. However, static aerodynamic characteristics have been successfully used as a guide in compensating for Reynolds number effects on dynamically-scaled, free spinning aircraft models[19].

The static stability of the SRC was measured at $Re_D = 0.9\times10^6$ in the ViGYAN subsonic wind tunnel[2]. Linear aerodynamic behavior was observed out to at least $\alpha = 28^0$. With the assumption of linear aerodynamic inputs and small damping, the static stability derivative $C_{m,\alpha}$ for an oscillating free-falling body can be estimated using the classical stability analysis employed in Ref. 3 from the equation;

$$C_{m,\alpha} = \frac{-\omega^2 I_y}{q_\infty AD} \tag{1}$$

Using this method the values in Table 5 are calculated using oscillation frequencies obtained directly from the angle-of-attack time history plots as well as the mass and geometric characteristics presented in Table 4. The boundary layer strakes were not installed on the model during these tests.

There is good agreement between the static stability derivative values based on static data measured at Re_D = 0.9×10^6 and those estimated using the dynamic data at 0.3×10^6. The static test Re_D in this comparison is still less than half of the flight value ($Re_D = 2.2\times10^6$ for the vehicle at terminal velocity at 10,000 ft altitude).

The authors are not aware of a definitive demonstration of the effect of Reynold's number on low subsonic dynamic stability of blunt configurations. In Ref. 9, Uselton examined the effect of varying Re_D from 0.4 to 1.2×10^6 on a 70 degree half-angle cone at Mach numbers between 1.9 and 2.65. He observed that the dynamic stability is, "... a strong function of Reynolds number and showed different trends at each Mach number. However, at $\alpha = 5.8^0$, ... the (dynamic stability) decreased slightly as Reynolds number increased." While the validity of this observation for low subsonic flows is unknown, this trend suggests that at the higher flight Reynolds numbers, the capsule is even less stable than measured in the present tests.

Modified Afterbody Geometries

In 1971, Ericson[14] concluded that,"The anomalous dynamic behavior of re-entry capsules is caused by separating and reattaching flows. ...(it) is the result of the finite time lag in the separated flowfield's response to the body cross-flow perturbations." In an attempt to alter the separation topology of the Stardust afterbody, two afterbody modifications were examined. These modifications were selected based on three criteria. First, there

Table 6: Equivalent Drag Areas for the Parachutes

Model Parachute Diameter in.	Equivalent Drag Area $C_D A_p$, ft^2
6.0	1.87
6.5	2.24
7.0	2.55
7.5	2.98

are size constraints on the capsule for integration into the host bus. Second, the intense aero-heating which the capsule must survive during the hypersonic portion of its entry require any modification to not introduce insurmountable thermal protection requirements (i.e. thin stabilizing fins are not acceptable.) Finally, because of the aft-location of center-of-gravity, the capsule also suffers a static instability in the hypersonic-free-molecular to hypersonic-rarefied flow regime (altitudes above 100 km). An afterbody modification was sought which would simultaneously fix both stability problems within size and thermal protection constraints of the mission.

The first modification is referred to as the "straight afterbody" and is shown in Fig. 8. It involves a cylindrical afterbody in place of the original cone. (The afterbody cylinder is recessed behind the maximum diameter point to aid in protecting a vehicle seal behind the shoulder.) The second modification is the "flared afterbody" depicted in Fig. 9. While a sufficiently large flare could have been added to create a dynamically stable configuration, the one shown in Fig. 9. represents the largest flare possible within the size constraints of the capsule.

The c.g. for both modified afterbody configurations was at 0.349 D. The full scale mass properties values converted from the scaled model were mass of 92.3 lb, I_x, I_y and I_z of 1.75, 1.33, and 1.27 slug-ft^2. Spin-tunnel tests revealed that neither modification eliminated the divergent growth of oscillations. As stated earlier, it is difficult to compare the degree of instability present in a divergent test. Observation of the afterbody tests, however, suggest that the "straight" afterbody modification may have delayed the oscillation growth while the "flared" modification may have exacerbated the motions.

Configuration with Parachutes

The addition of a stabilizing parachute is examined next. The Mercury and Gemini capsules both deployed stabilizing parachutes before main parachute deployment[20,21].

The size of the parachute necessary to stabilize the vehicle is dependent on the extent of instability. Larger parachutes possess more drag which results in higher tow line tensions and lower descent velocities. Lower velocities are accompanied by lower dynamic pressures which decreases the magnitude of the destabilizing aerodynamic forces. Higher tow line tension, when transmitted through the bridle to vehicle, causes the vehicle to "hang" from the bridle in a stable orientation.

Initial tests revealed that the addition of parachutes as small as 3.0 inches in diameter (full scale drag area of 0.47 ft^2) could result in a vehicle which could maintain a controlled attitude. However, the arrangement was conditionally stable. If a sufficiently large perturbation was introduced, the vehicle could still tumble. In all probability, there exists a perturbation threshold below which the 3.0 inch parachute system is stable. As parachute size increases, this threshold would likewise increase. In a free-flight testing environment it is difficult to introduce precise, repeatable perturbations to establish this threshold. The objective of the tests was modified to find the smallest parachute which could damp out a large perturbation.

Four round parachutes with diameters from 6.0 inches to 7.5 inches were examined. Equivalent full scale drag areas are presented in Table 5. The parachutes were attached to the vehicle's stern with a three point bridle. The diameter of the model's bridal arrangement was 2.14 inches which corresponds to the flight vehicle's 9.0 inch parachute tray. The bridal was 4 inches long (corresponding to 17 inches for flight) and the length from vehicle to canopy was 10 vehicle diameters.

To introduce a large but repeatable attitude perturbation for this study the vehicle was hand launched into the flow upside down beneath a fully deployed parachute. In particular, the test technician held the vehicle

upside down as the parachute fills overhead. When the tunnel velocity was sufficient to support the vehicle, it was released. This procedure typically introduced initial angle-of-attack oscillations around 90 degrees.

For the 7.5, 7.0, and 6.5 inch diameter parachutes, this large oscillation damped out for every launch. For the 6.0 inch chute, the vehicle established itself in a non-decaying oscillation with amplitude of 90 degrees. Occasionally, a combination of angle of attack, sideslip, and bridal orientation occured which eliminated the large oscillation and the vehicle stabilized. On one occasion, however, a different combination induced a catastrophic spin which was not recovered before contact with the tunnel capture net. The 6.0 inch parachute was judged too small to damp large oscillations.

Conclusions

Successful return of interstellar dust and cometary material by the Stardust Sample Return Capsule requires that the capsule maintain a controlled flight attitude through the subsonic portion of the trajectory. Dynamic stability testing in the NASA 20-Foot Vertical Spin Tunnel was used to assess the vehicle's dynamic stability in this flight regime. The original design was found to be dynamically unstable at low subsonic conditions due to the aft-location of its center-of-gravity at 0.35 body diameters from the nose. The divergent behavior of the capsule continued when the center-of-gravity was moved to 0.337 and 0.313 body diameters back from the nose. When the center-of-gravity was moved further forward to 0.29 body diameters back from the nose, the vehicle established itself in a limit cycle with amplitude around 10 degrees. The higher Reynolds numbers associated with the actual flight might require the center-of-gravity to be even closer to the nose.

Modifying the afterbody from its original conical shape to a cylinder or a flare did not eliminate the divergent oscillations when the center-of-gravity was 0.35 body diameters back from the nose.

The addition of a parachute can stabilize the vehicle. The parachute must be at least 6.5 inches in diameter for the model, or an equivalent full scale drag area, $C_D A_p$, of 2.24 ft^2 for the flight vehicle, to assure large perturbations are damped.

Acknowledgments

Mr. Thomas Abbott of the Fabrication Division was responsible for the construction of the test model.

References

[1]Atkins, K. L.; Brownlee, D. E.; Duxbury, T.; Yen, C.; and Tsou, P.:"STARDUST: Discovery's Interstellar Dust and Cometary Sample Return Mission," Proceedings from the 1997 IEEE Aerospace Conference, Feb., 1997.

[2]Mitcheltree, R. A.; Wilmoth, R. G.; Cheatwood, F. M.; Rault, D. A.; Brauckmann, G. J.; and Greene, F. A.: "Aerodynamics of Stardust Sample Return Capsule," AIAA Paper 94-2304, June, 1997.

[3]Bendura, R. J.:"Low Subsonic Static and Dynamic Stability Characteristics of Two Blunt 120^0 Cone Configurations," NASA TN D-3853, Feb., 1967.

[4]Costigan, P. J.:"Dynamic-Model Study of Planetary-Entry Configurations in the Langley Spin Tunnel," NASA TN D-3499, July, 1966.

[5]Cahen, G. L.: "Effects of Shape and Mass Properties on Subsonic Dynamics of Planetary Probes," *Journal of Spacecraft and Rockets*, Vol. 12, No. 8, Aug., 1975.

[6]Marte, J. E.; and Weaver, R. W.:"Low Subsonic Dynamic-Stability Investigation of Several Planetary-Entry Configurations in a Vertical Wind Tunnel (Part I)," JPL TR 32-743, May, 1965.

[7]Jaffe, P.:"Terminal Dynamics of Atmospheric Entry Capsules," *AIAA Journal*, Vol. 7, No. 6, June, 1969.

[8]Marko, W. J.:"Transonic Dynamic and Static Stability Characteristics of Three Blunt-Cone Planetary Entry Shapes," NASA CR-107405, JPL TR 32-1357, Sept., 1969.

[9]Uselton, B. L.; Shadow, T. O.; and Mansfield, A. C.: "Damping in Pitch Derivatives of 120 and 140 Deg Blunted Cones at Mach Numbers 0.6 through 3.0," AEDC TR-70-49, 1970.

[10]Cassanto, J. M.; and Buce, P.:"Free Fall Stability and Base Pressure Drop Tests for Planetary Entry Configurations," *Journal of Spacecraft and Rockets*, Vol. 8, No. 7, July, 1971.

[11]Jaffe, P.:"Dynamic Stability Tests of Spinning Entry Bodies in the Terminal Regime," *Journal of Spacecraft and Rockets*, Vol. 8, No. 6, June, 1971.

[12]Whitlock, C. H.; and Bendura, R. J.:"Dynamic Stability of a 4.6-meter Diameter 120^0 Conical Spacecraft at Mach Numbers From 0.78 to 0.48 in a Simulated Martian Atmosphere," NASA TN D-4558, May, 1968.

[13]Krumins, M. V.: "A Ballistic Range Study of the Aerodynamic Characteristics of Mars Probe/Lander Shapes," AIAA Paper 67-167, Jan., 1967.

[14]Ericson, L. E.; and Reding, J. P.:"Re-Entry Capsule Dynamics," *Journal of Spacecraft and Rockets*, Vol. 8, No. 6, June, 1971.

[15]Shirley, D. L.; and Masselhorn, J. E.:"Instability of High-Drag Planetary Entry Vehicles at Subsonic Speeds," *Journal of Spacecraft and Rockets*, Vol. 5, No. 10, Oct., 1968.

[16]Neihouse, A. I.; Kliner, W. J.; and Scher, S. H.:"Status of Spin Research for Recent Airplane Designs," NASA TR R-57, 1960.

[17]Snow, W. L.; Childers, B. A.; Jones, S. B.; and Fremaux, C. M.:"Recent Experiences with Implementing a Video Based Six Degree of Freedom Measurement System for Airplane Models in a 20-Foot Diameter Vertical Spin Tunnel," Proceedings of the SPIE Videometrics Conference, Vol. 1820, 1992, pp. 158-180.

[18]Wolowicz, C. H.; Bowman, J. S.; and Gilbert, W. P.:"Similitude Requirements and Scaling Relationships as Applied to Model Testing," NASA TP 1435, 1979.

[19]Whipple, R. D.; and Ricket, J. L.:"Low-Speed Aerodynamic Characteristics of a 1/8-Scale X-29A Airplane Model at High Angles of Attack and Sideslip," NASA TM 87722, 1986.

[20]Bowman, J. S.: "Dynamic Model Tests at Low Subsonic Speeds of Project Mercury Capsule Configurations with and without Drogue Parachutes," NASA TM X-459, 1963.

[21]Lee, H. A.; Costigan, P. J.; and Bowman, J. S.:"Dynamic-Model Investigation of a 1/20-Scale Model of the Gemini Spacecraft in the Langley Spin Tunnel," NASA TN D-2191, 1964.

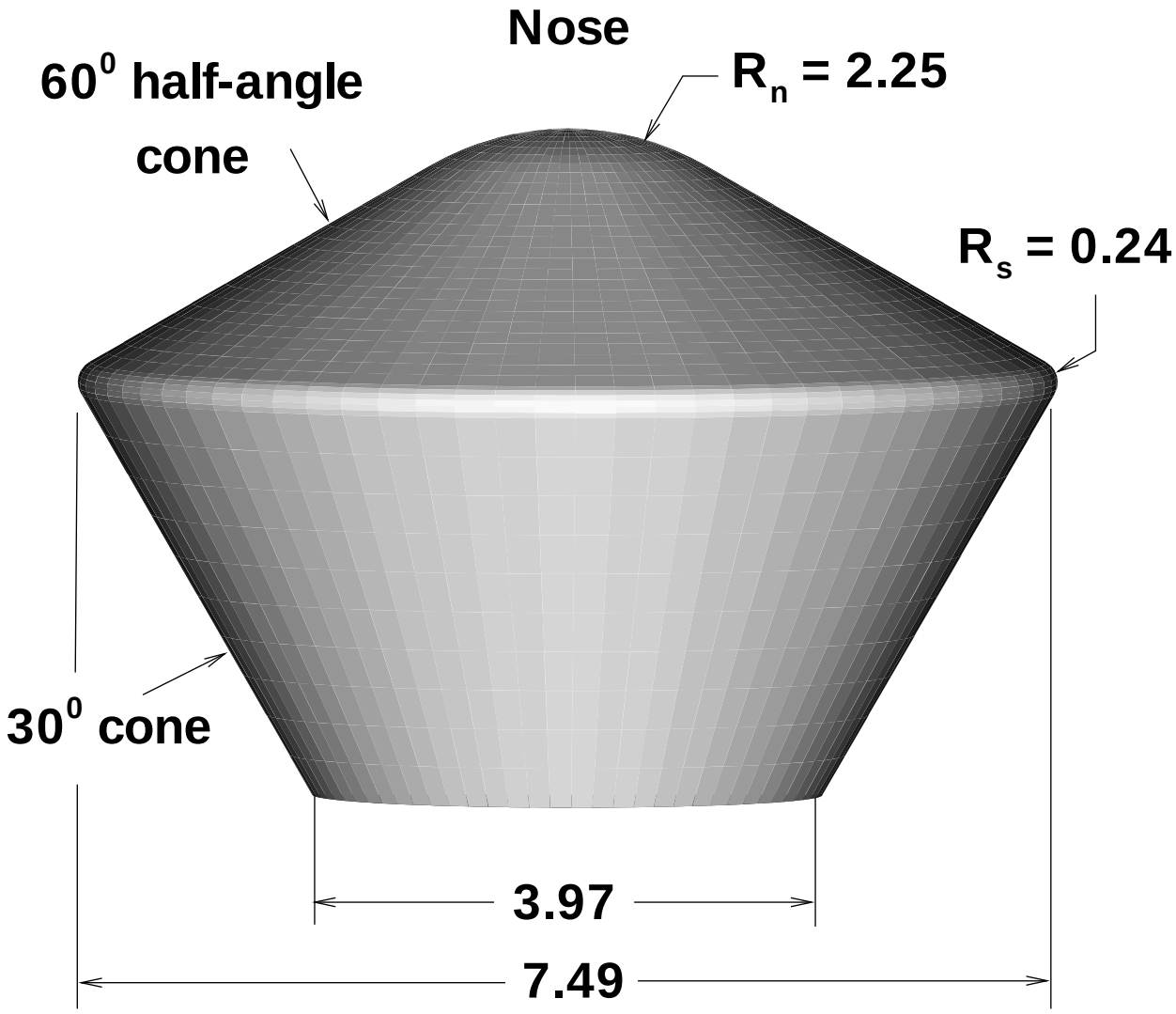

Figure 1. Stardust SRC 23.8% Spin Tunnel model geometry (in inches).

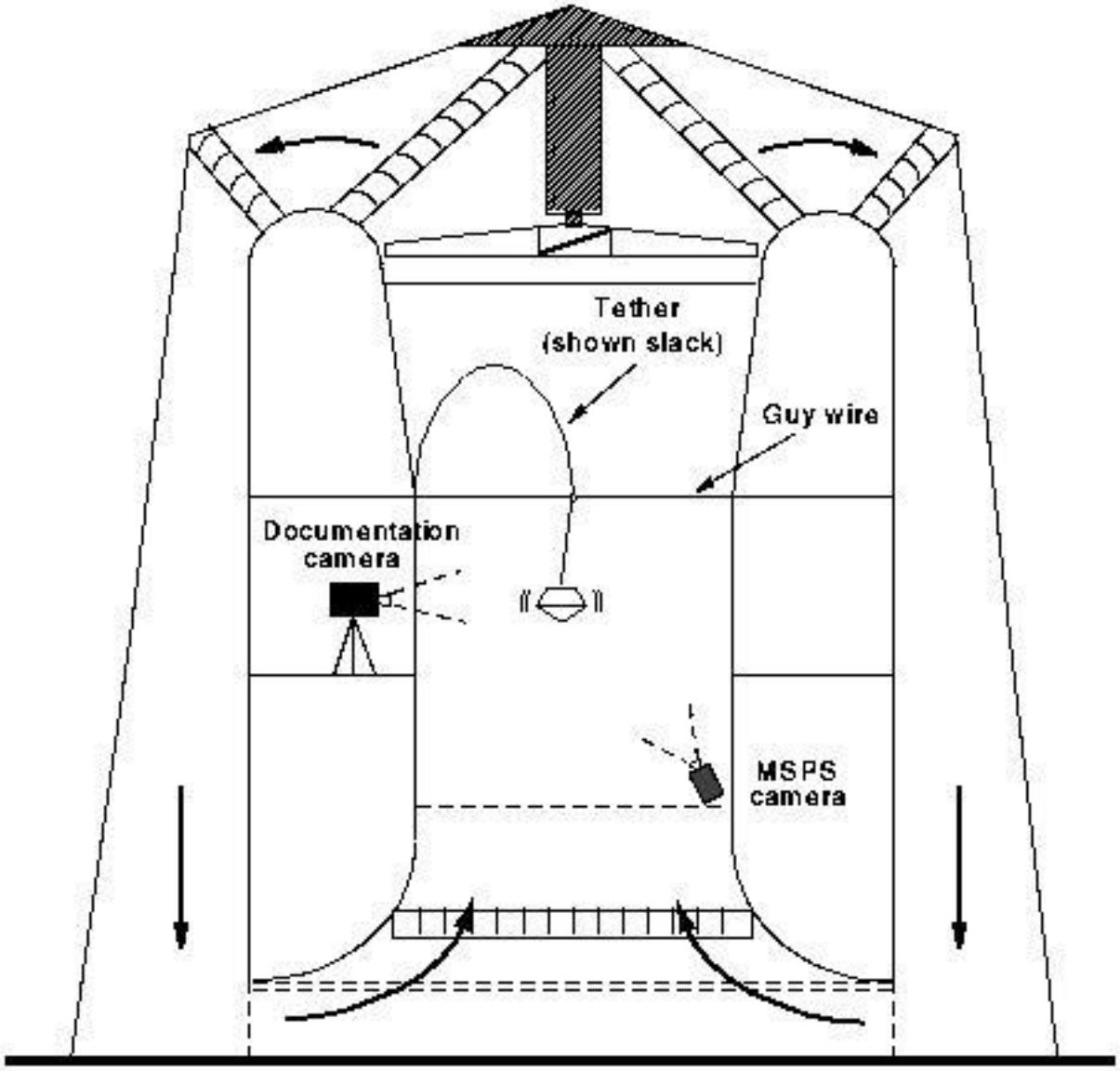

Figure 2. Cross section of the NASA Langley 20-Foot Vertical Spin Tunnel with 23.8%-scale Stardust model installed on tether system.

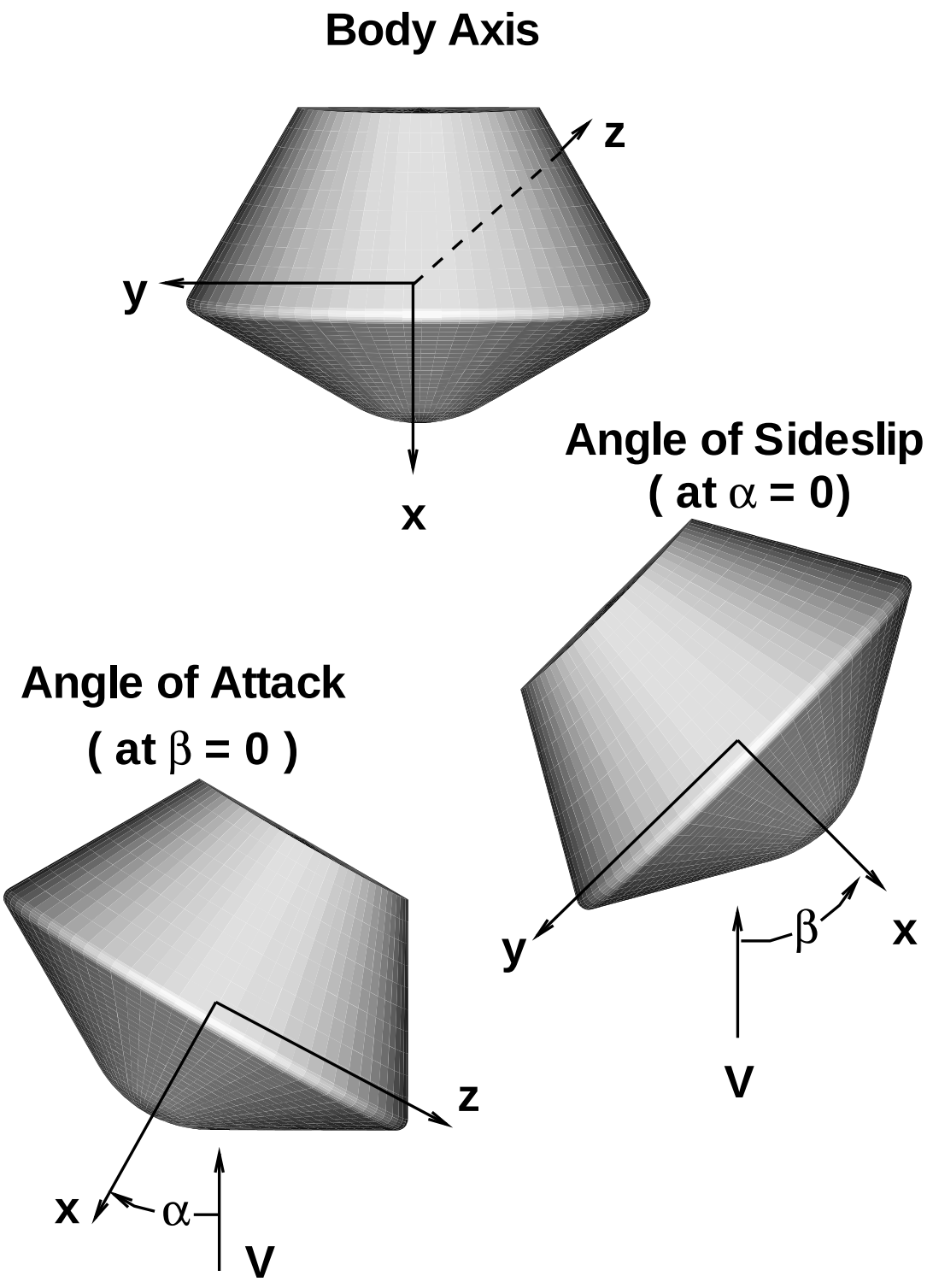

Figure 3. Axis System and aerodynamic angle definitions used in dynamic stability tests in the 20-foot Vertical Spin Tunnel.

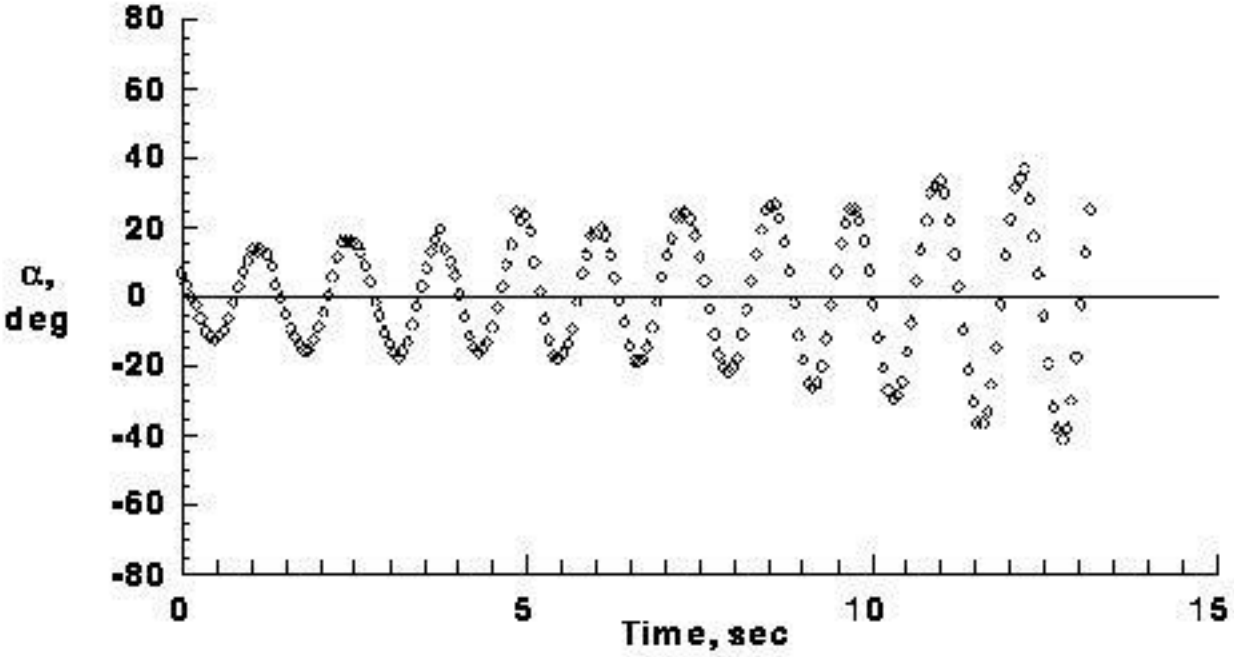

(a) angle of attack

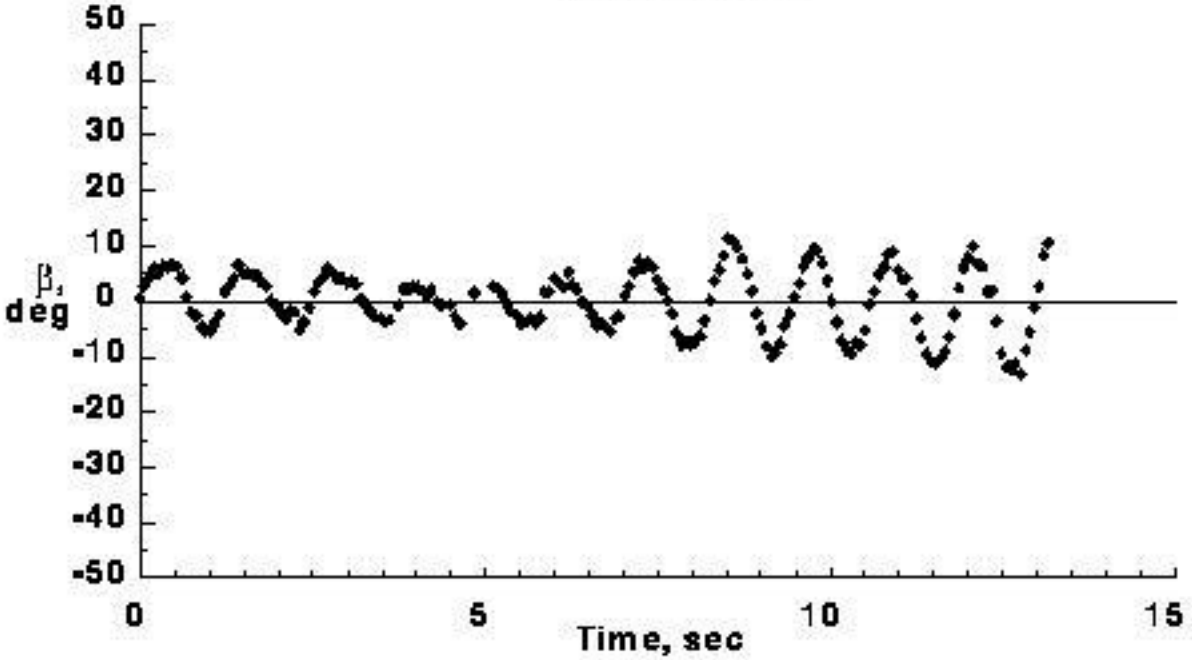

(b) angle of sideslip

Figure 4. Motion time history of 23.8%-scale Stardust model in the 20-Foot Vertical Spin Tunnel. Center of gravity at $X_{C.g.}/D$ of 0.351. Values are full-scale converted from model scale.

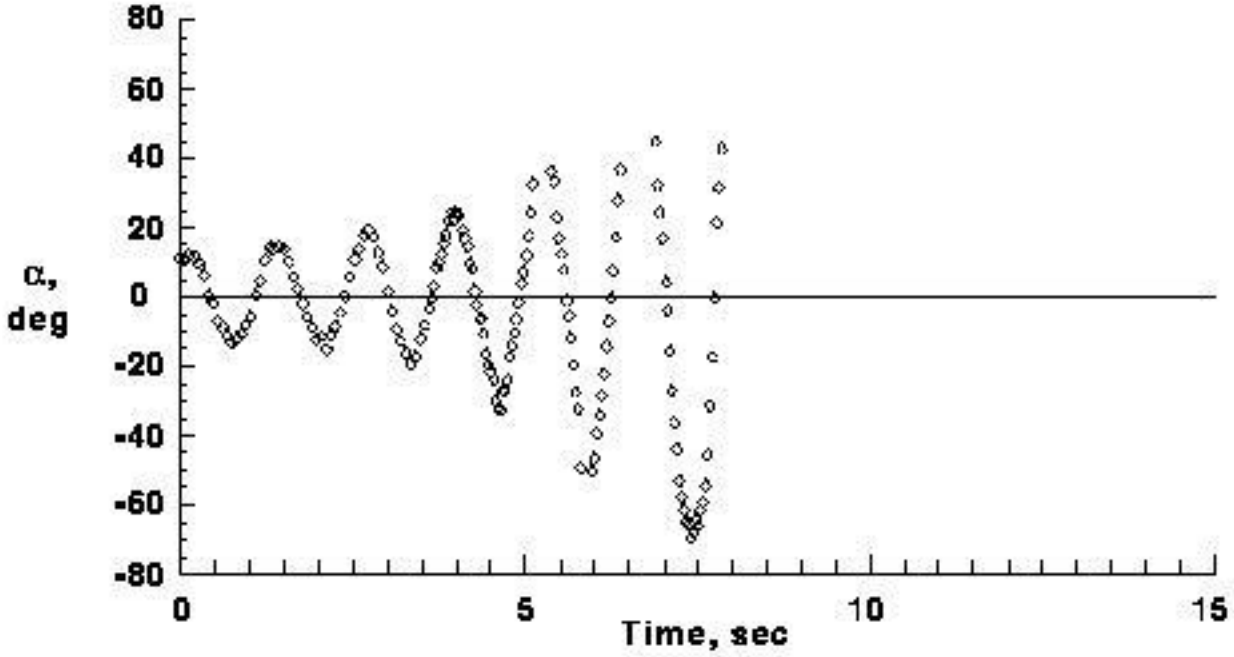

(a) angle of attack

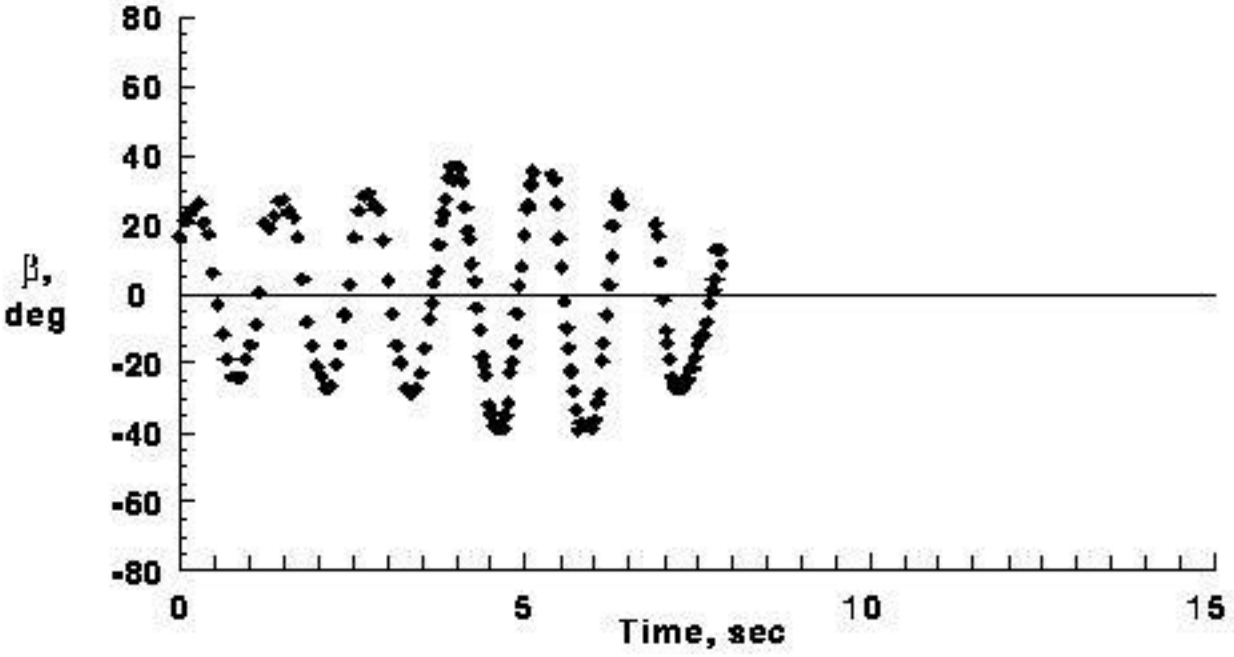

(b) angle of sideslip

Figure 5. Motion time history of 23.8%-scale Stardust model in the 20-Foot Vertical Spin Tunnel. Center of gravity at $X_{c.g.}/D$ of 0.337. Values are full-scale converted from model scale.

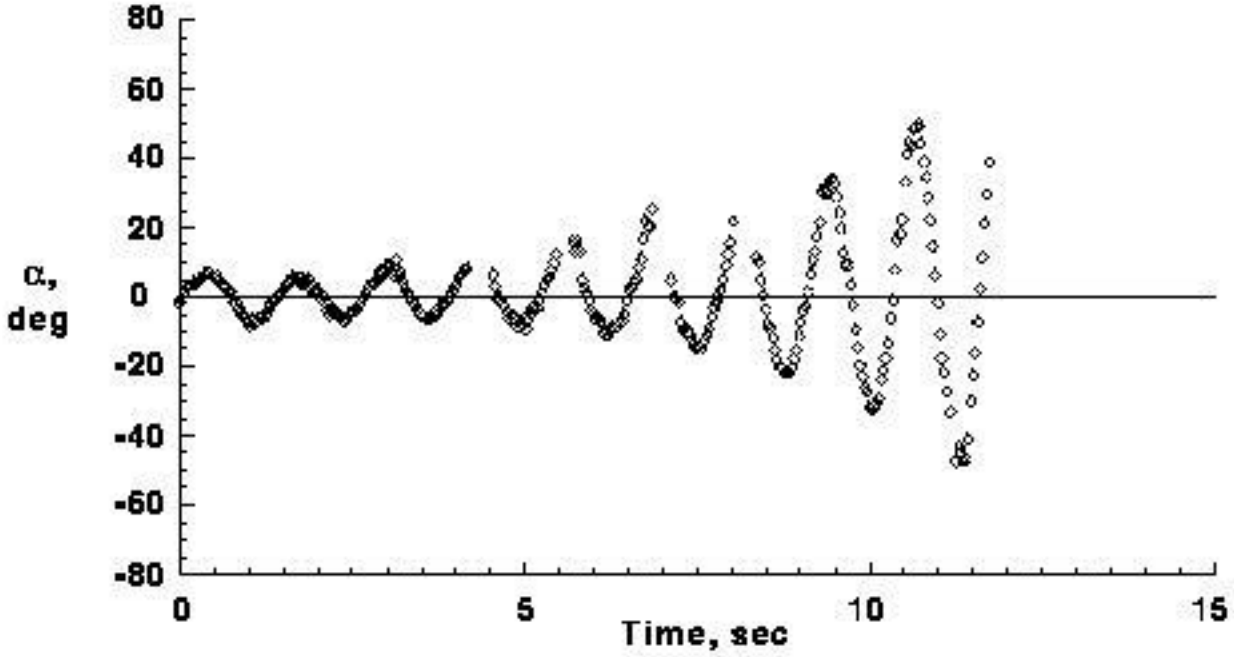

(a) angle of attack

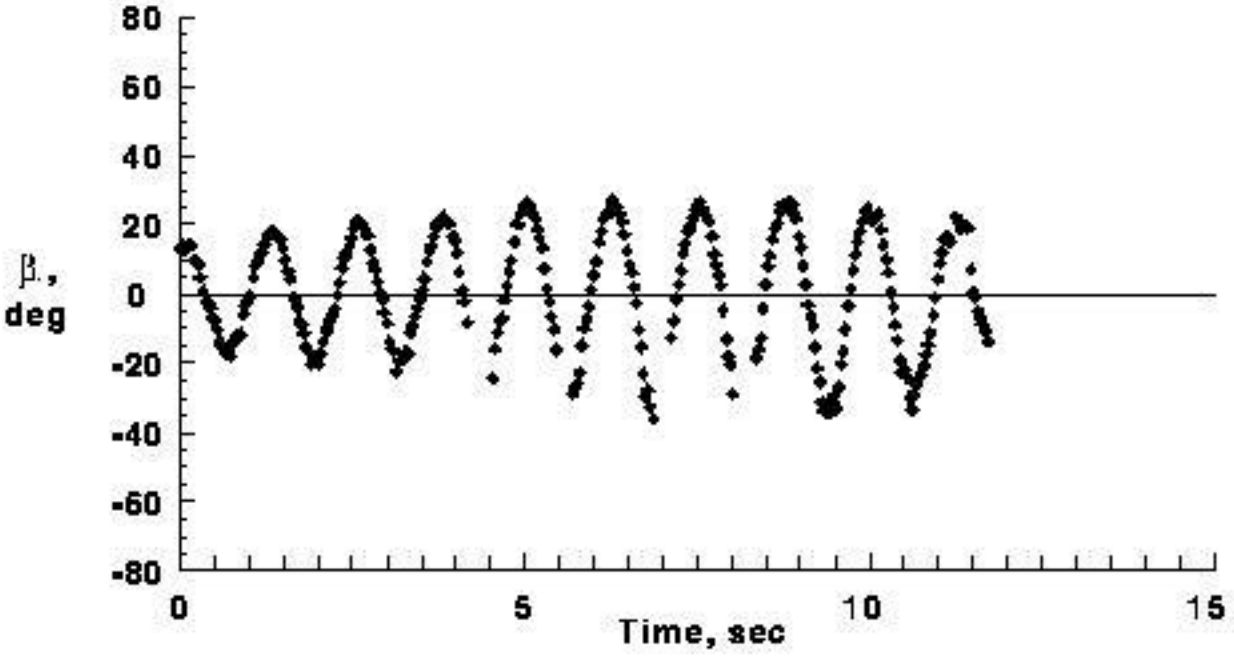

(b) angle of sideslip

Figure 6. Motion time history of 23.8%-scale Stardust model in the 20-Foot Vertical Spin Tunnel. Center of gravity at $X_{c.g.}/D$ of 0.313. Values are full-scale converted from model scale.

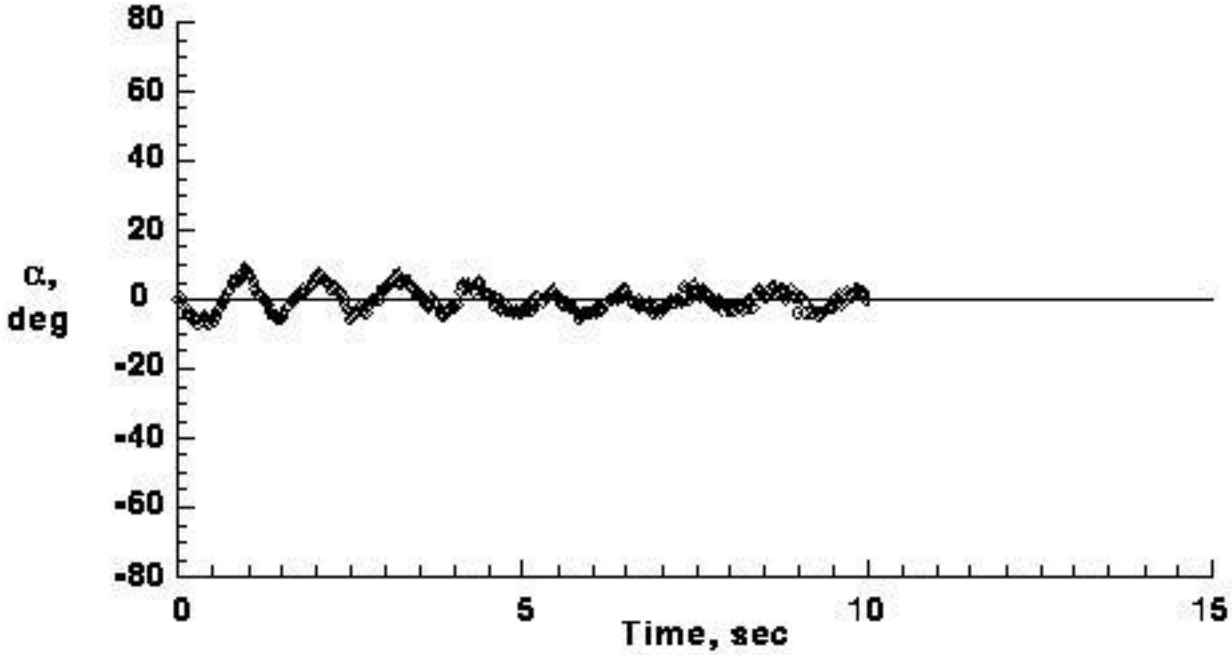

(a) angle of attack

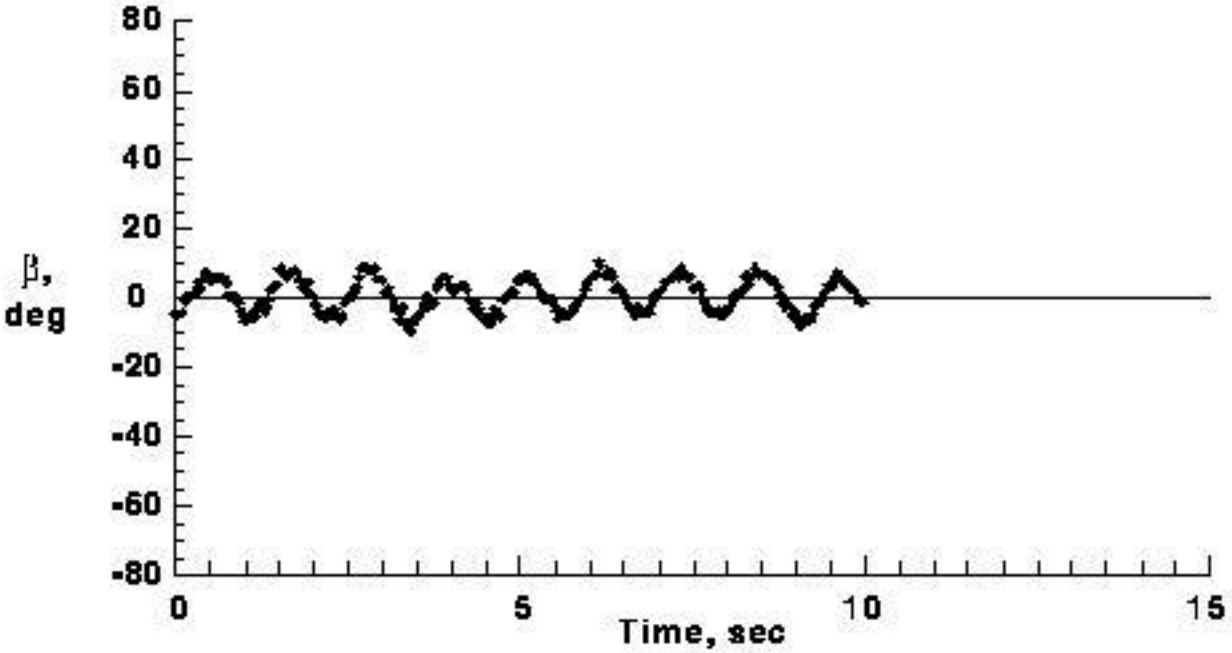

(b) angle of sideslip

Figure 7. Motion time history of 23.8%-scale Stardust model in the 20-Foot Vertical Spin Tunnel. Center of gravity at $X_{c.g.}/D$ of 0.290. Values are full-scale converted from model scale.

Straight Afterbody Modification

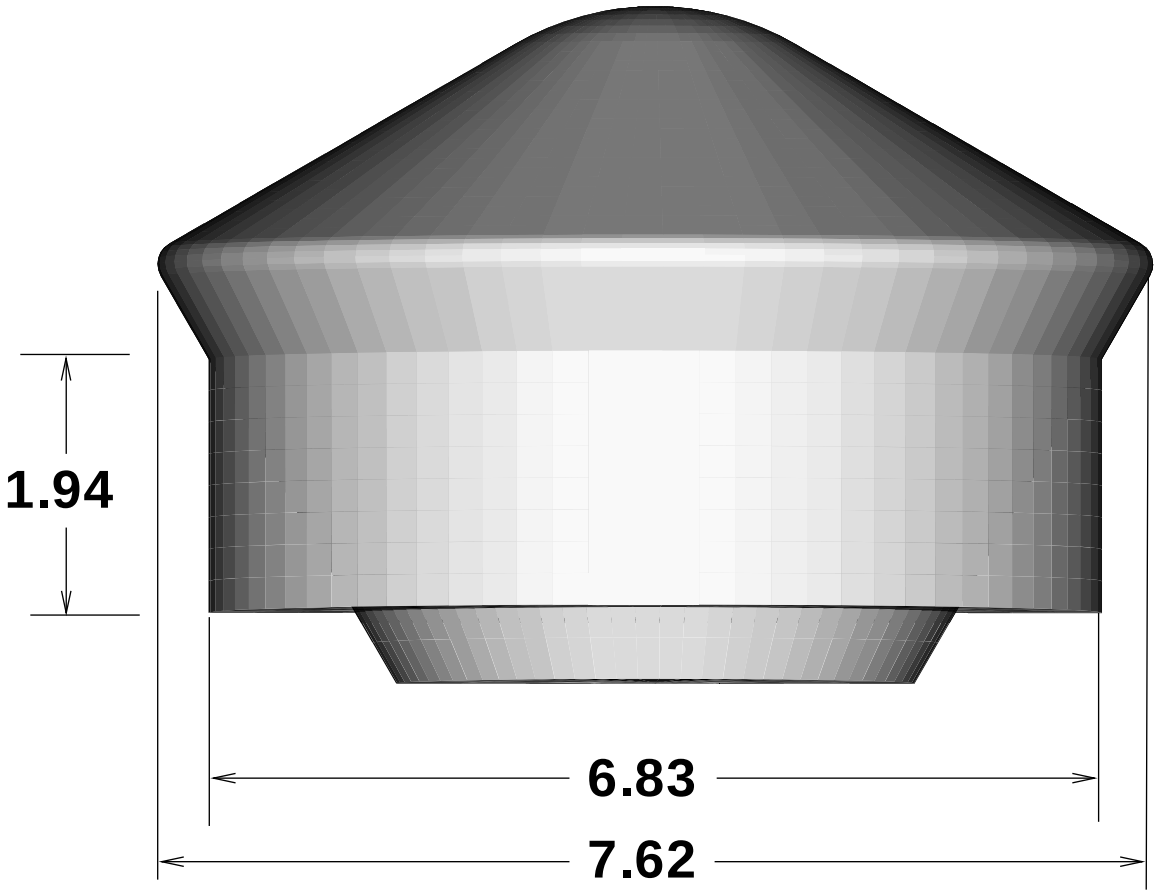

Figure 8. Straight afterbody modification to SRC Spin Tunnel model (in inches).

Flared Afterbody Modification

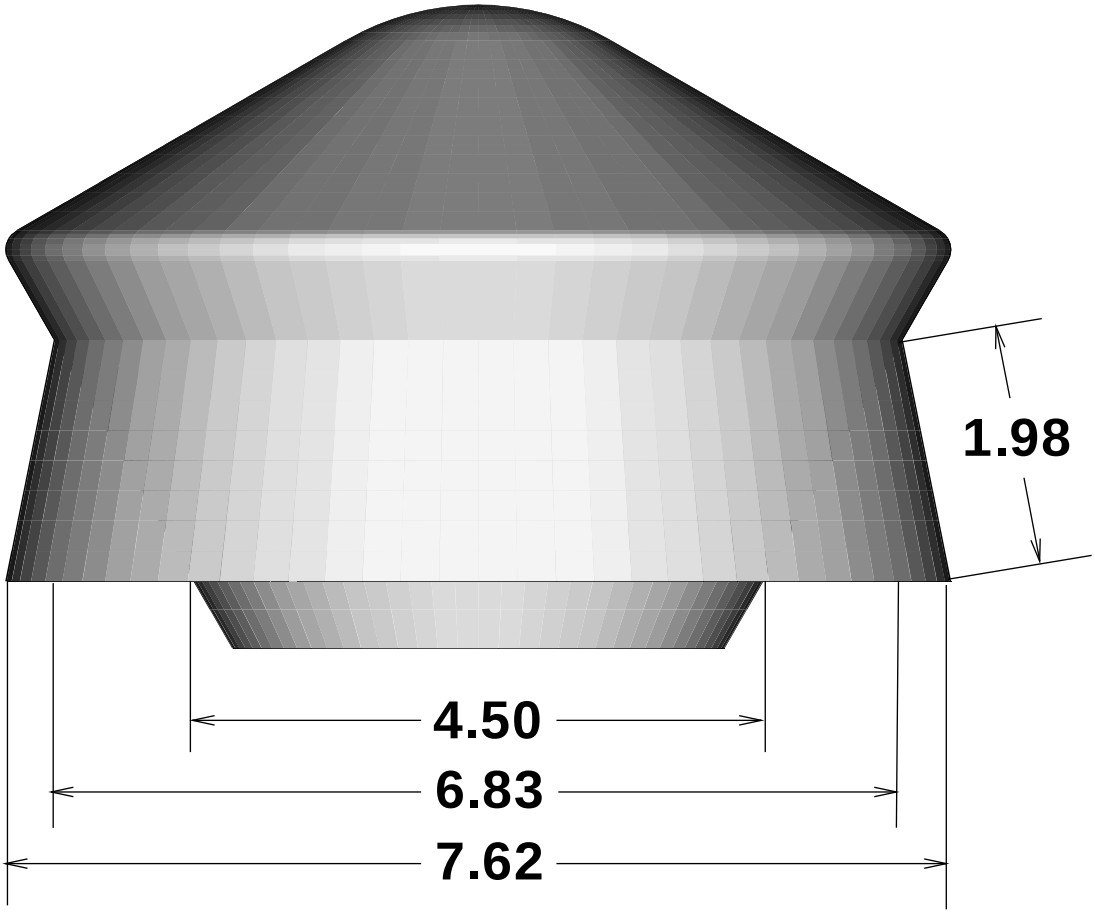

Figure 9. Flared afterbody modification to SRC SpinTunnel model (in inches).